DOI: 10.13009/EUCASS2019-528



# Transient Model of API Injector Using EcoSimPro for Expander Bleed Engine Application

R. H. S. Hahn*[1], I. D. Hoffmann[1], J. Deeken[1], M. Oschwald[1], S. Schlechtriem[1]
[1]*German Aerospace Center DLR, Institute of Space Propulsion, Germany*
*robson.dossantoshahn@dlr.de

## Abstract

API injector system has been investigated in DLR Lampoldshausen for the last decade and has been proved to be a reliable design for LOx/LH2 engines. In this work will be presented the transient models of an API injector using EcoSimPro with ESPSS library and the system evaluation in different design conditions as well as the model validation using an already known design from in house test subject and an insight of future application of such design applied in in the LUMEN expander bleed demonstration engine.

## 1. Introduction

Within framework of LUMEN project (Liquid Upper stage deMonstrator ENgine), which consist in an engine demonstrator in development and foreseen to be tested at DLR Lampoldshausen within the capabilities of P8 test stand, the requirements were defined in order to fulfil the design needs and estimate the detailed design constrains for the cycle prediction and its transient evaluation based on a defined architecture.
For the LUMEN demonstrator, the utilization of LNG targets the system simplification, which trade-offs shows to provide advantages over LH2, as higher specific density, minimum temperature difference between fuel and oxidizer, etc.
The use of LNG, which in this application is contains above 98% of Methane results in a system with a negative point for performance due to a turbine driver fluid with adiabatic specific work in lower range than a gas generator driven system with maximum turbine driven temperature limited by the thermal design of a regenerative cooling subsystem. Thus, the heat transfer plays an important role in the system design.
Despite performance not be a primary objective for LUMEN Demonstrator, the use of Advanced Porous Injector (API) provides advantage for the cycle due its heat release behavior [1][2][3] compared to shear coaxial injectors, commonly used in expander bleed cycle [5][6].
In order to correctly evaluate the design and simulate the transient behavior of LUMEN demonstrator, the use of simplified injector models can lead to systematic errors for cycle analysis in design (steady-state conditions) as well as transient analysis, which plays an important role on cycle feasibility as well as fulfilment of operational conditions.

## 2. Flow through porous media

Various models available can predict the flow through a porous media in different operational regimes. For a LRE, however, the thermodynamic conditions as well as the fluid properties are not deeply investigated, especially when in use the porous media as the injection system, where the transport properties, flow velocity, pressure and temperature ranges are far from most studies available. The main theory used for evaluate flow in porous materials are presented as follows.

### 2.1. Darcy's Law

Initial investigations from Henry Darcy [7] have shown the linear relationship between the flowrate through a porous bed and the pressure drop and are based on conservation of momentum. This linear relationship is known today as Darcy's Law and is shown at the Equation (1) and (2).

DOI: 10.13009/EUCASS2019-528



$$Q = -\frac{K \cdot A \cdot \Delta P}{\mu_f \cdot L} \tag{1}$$

$$\nabla P = -\frac{\mu_f \cdot u_D}{K} \tag{2}$$

The Darcy's Law, however, has validity for low speed flow, where is generally used for modelling petroleum reservoirs and aquifers, therefore only accounts for the viscous resistance of the flow.

## 2.2. Forchheimer

For high speed flows, where the inertial contributions become noticeable, the use of Forchheimer is preferable. The simplified model can be represented in the equation **(3)**

$$\nabla P = -\frac{\mu_f \cdot u_D}{K} - \frac{\mathrm{C}_f \cdot \rho \cdot u_D^2}{\sqrt{K}} \tag{3}$$

Where $\mathrm{C}_f$ is known as Forchheimer (Non-Darcian) coefficient. Originally $\mathrm{C}_f$ was taken as constant and approximately 0,55. However, later studies have shown that it varies with different porous media, as seen in a study for flow over spheres [8], as presented in the equation **(4)**

$$\mathrm{C}_f = 0{,}55 \cdot \left(1 - 5{,}5 \cdot \frac{S_d}{D}\right) \tag{4}$$

Where $S_d$, is the sphere diameter and $D$ the porous plate diameter.
In this work, the Forchheimer equation can also be rewritten in function of terms $\alpha$ and $\beta$ respectively for viscous and inertial part of the equation, as shown in the equation **(5)**.

$$\nabla P = -\frac{\mu_f \cdot u_D}{\alpha} - \frac{\rho \cdot u_D^2}{\beta} \tag{5}$$

The term a is equivalent to the specific permeability, while b is the Non-Darcian coefficient with regarding the Darcy's Law, as shown respectively at the equations (6) and **(7)**.

$$\alpha = K \tag{6}$$

$$\beta = \frac{\sqrt{K}}{0{,}55 \cdot \left(1 - 5{,}5 \cdot \frac{S_d}{D}\right)} \tag{7}$$

Those coefficients can only be found empirically [9]. However, this additional inertial resistance can be caused by different mechanisms [10] as turbulence, Microscopic Inertial Forces and Increased microscopic drag forces.

## 2.3. Erguns Model

The Erguns model was created in 1952 [11] to solve the lack of parameters correlating the porous media in Forchheimer model, resulting in parameters $\alpha$ and $\beta$ as a function of the media rather than a universal constant. This resulted in the implementation of direct parameter for the medium porosity as $\epsilon$, the diameter of the porous media as $D$ and two constants here as $A$ for the viscous-dominated part and $B$ for the inertial-dominated part and are respectively 150 and 1,75, as seen in the equation (8).

$$\nabla P = -\frac{\mu_f \cdot 150 \cdot (1-\epsilon)^2 \cdot u_D}{\epsilon^3 \cdot D^2} + \frac{\rho \cdot 1{,}75 \cdot (1-\epsilon) \cdot u_D^2}{\epsilon^3 \cdot D} \tag{8}$$

DOI: 10.13009/EUCASS2019-528



Therefore, the Erguns equation can be also implemented in the Forchheimer model. Thus, the values for $\alpha$ and $\beta$ used by Ergun's equation can be shown in the Equation (9) and (10) respectively.

$$\alpha = \frac{\epsilon^3 \cdot D^2}{A \cdot (1-\epsilon)^2} \tag{9}$$

$$\beta = \frac{\epsilon^3 \cdot D}{B \cdot (1-\epsilon)} \tag{10}$$

### 2.4. Carman-Kozeny

Finally, for the correction of the porosity dependence on the Ergun's Equation, the model was modified in order to use a correction factor, empirically tested for engineering purposes, based on the particles quality of the porous media, called Carman-Kozeny Equation. The parameter $A$ was adopted as 180 units while $B$ is assumed to be a function of particle or wall roughness which value lies between 1,8 and 4,0 [12][8].

## 3. EcosimPro Model

In order to evaluate the transient behavior of a porous injector head, the Carman-Kozeny and Forchheimer equations was implemented in a code to evaluate the pressure drop according to the mass flow rate through the porous media. Initial standard parameters for both models were used initially, followed by different approaches to evaluate the flow resistance in the porous media. The following sections present the particularities for each of the models developed for the API injector according to experimental results from previous tests carried at DLR Lampoldshausen [1].

### 3.1. Alpha Infinite

In this approach, the standard Forchheimer equation (5) was used. This method assumed that the first term of equation provides no contribution for the pressure loss in the system, while only the inertial part of the equation contributes to the injector head resistivity.
This method was used previously by DLR in this field of study with Rigimesh porous media and has proven to provide results with enough precision in some operational condition ranges rated for LRE application.

### 3.2. Alpha Infinite with Beta Variable

The method presented at item 3.1 can show deviation in range of 40% for some extreme test cases. Therefore, in order to use the same approach, the term β was adopted as a variable in function of fluid properties though the porous media.

$$\beta = F \cdot {R_e}^G \tag{11}$$

The correlation from equation (11) is based in experimental data and the parameters F and G correlates with the porosity and plate thickness respectively. Thus, the new Forchheimer Equation used in this model, can be seen in the Equation (12) .

$$\nabla P = -\frac{\rho \cdot u_D^2}{F \cdot {R_e}^G} \tag{12}$$

### 3.3. Alpha and Beta

While the approaches presented in the item 3.1 and 3.2 can be used to represent the Rigimesh faceplate, the use of sintered bronze [13] requires the use of finite $\alpha$ parameter. Since the test data was created using metallic mesh face plate, this approach was only investigated in its modified form as follows.

DOI: 10.13009/EUCASS2019-528



### 3.4. Alpha and Beta with Beta Variable

In a similar approach as presented for item 3.2, the need to precise evaluate the sintered bronze [13] porous injector plate, the $\beta$ term was also adopted as a function of Reynolds. Once more, the terms $F$ and $G$ was used to describe the correlation with the porosity and plate thickness respectively and was obtained according to experimental data from test campaign at DLR Lampoldshausen. This approach only takes $\beta$ as variable due to its bigger influence in the pressure loss due to the $u_D^2$ term and is shown at the equation (13).

$$\nabla P = -\frac{\mu_f \cdot u_D}{\alpha} + \frac{\rho \cdot u_D^2}{F \cdot {R_e}^G} \tag{13}$$

### 3.5. Carman-Kozeny

For this injector model the Carman-Kozeny equation was used. The advantage of this model is that it can be used with any porous material, including Rigimesh, Sintered Bronze, 3D printed face plate and other possibilities due to the term $\epsilon$ which is responsible for the porosity in the material.
The simplified approach of Carman-Kozeny in this implementation uses $CK_{f1}$ and $CK_{f2}$ with the values of 180 and 1,80 respectively. The $CK_{f2}$ value chosen for this model was 1,80 as an acceptable approach according to [12] as seen in the Equation (14).

$$\nabla P = -\frac{\mu_f \cdot 180 \cdot (1-\epsilon)^2 \cdot u_D}{\epsilon^3 \cdot D^2} + \frac{\rho \cdot 1{,}80 \cdot (1-\epsilon) \cdot u_D^2}{\epsilon^3 \cdot D} \tag{14}$$

### 3.6. Carman-Kozeny with $CK_{f2}$ Variable

In order to improve the results from the model shown in the item 3.5, $CK_{f2}$ was set to be a variable dependent of the Reynold number. Initial analyses shown the range of $CK_{f2}$ between 1,80 and 4,00 for hydrogen injection at the operational envelope tested at DLR Lampoldshausen. This approach can rewrite the Carman-Kozeny equation as shown in the equation (15).

$$\nabla P = -\frac{\mu_f \cdot 180 \cdot (1-\epsilon)^2 \cdot u_D}{\epsilon^3 \cdot D^2} + \frac{\rho \cdot F \cdot {R_e}^G \cdot (1-\epsilon) \cdot u_D^2}{\epsilon^3 \cdot D} \tag{15}$$

Where, once more, the parameters $F$ and $G$ correlates with the porosity and plate thickness respectively and was obtained experimentally.

### 3.7. Reynolds Dependency

A simplified model was implemented using one single exponential equation which assumes that not only a, but also b and the porosity would be incorporated in the dependency. This approach, presented at equation (16), is result of experimental analysis and evaluation of the pressure resistance behavior according to the flow media properties during the tests. The next step in this model is evaluating the main influence of the obtained parameters according to the different porous media, geometry and flow.

$$\nabla P = H \cdot e^{I \cdot R_e} \tag{16}$$

## 4. Results

In order to validate the models presented, an EcosimPro experiment was created and the combustion chamber was simulated, using the boundary conditions as the test results, as the mass flow rate and fluid properties from the experimental data.
As for the data, main test cases from calorimetric combustion chamber using API injector head, tested in 2012 and 2013 were used for validation [1]. The chamber pressure ranged from 4,0MPa to near to 12,0MPa, with injection temperature in the range of 80K to 110K.

DOI: 10.13009/EUCASS2019-528



The nomenclature description associated to the test case and the data range is presented the Table 1.

Table 1 – Correlation of nomenclature with the test case and data range

| Load Point | Test Case | Data range |
|---|---|---|
| 1A | CALO 01 | 06s – 10s |
| 2A | CALO 01 | 13s – 18s |
| 3A | CALO 01 | 20s – 25s |
| 4A | CALO 01 | 27s – 32s |
| 5A | CALO 01 | 34s – 39s |
| 6A | CALO 01 | 41s – 46s |
| 7A | CALO 01 | 50s – 53s |
| 1B | CALO 02 | 06s – 10s |
| 2B | CALO 02 | 13s – 18s |
| 3B | CALO 02 | 20s – 25s |
| 4B | CALO 02 | 27s – 32s |
| 5B | CALO 02 | 34s – 39s |
| 6B | CALO 02 | 41s – 46s |
| 7B | CALO 02 | 50s – 53s |
| 1C | CALO 03 | 06s – 10s |
| 2C | CALO 03 | 13s – 18s |
| 3C | CALO 03 | 20s – 25s |
| 4C | CALO 03 | 27s – 32s |
| 5C | CALO 03 | 34s – 39s |
| 6C | CALO 03 | 41s – 46s |
| 7C | CALO 03 | 50s – 53s |

To simulate the experiment, an EcosimPro model using ESPSS library and the modified combustion chamber with utilization of different options of porous media models was created. The model, as presented at the Figure 1 was simplified in order to optimize the computational time and facilitate the convergence

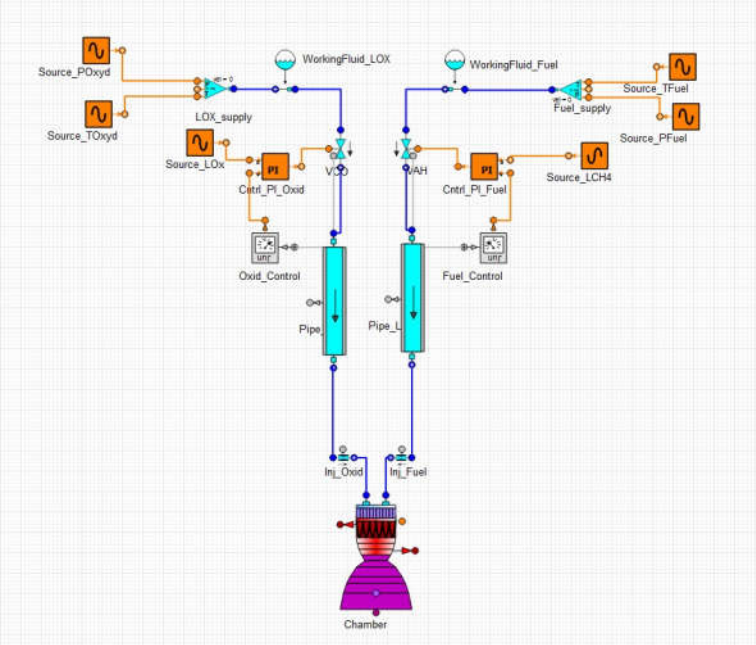


Figure 1: EcosimPro/ESPSS model of CALO experiment with focusing in the API/Chamber section and imposed boundary conditions

DOI: 10.13009/EUCASS2019-528



The results of simulation using the previously described main models are shown as follows.

### 4.1. Alpha Infinite

The standard model shown considerable proportional deviation between the other proposals. The main reason is related to the omission of the first term of equation (5), as is shown on Figure 2.

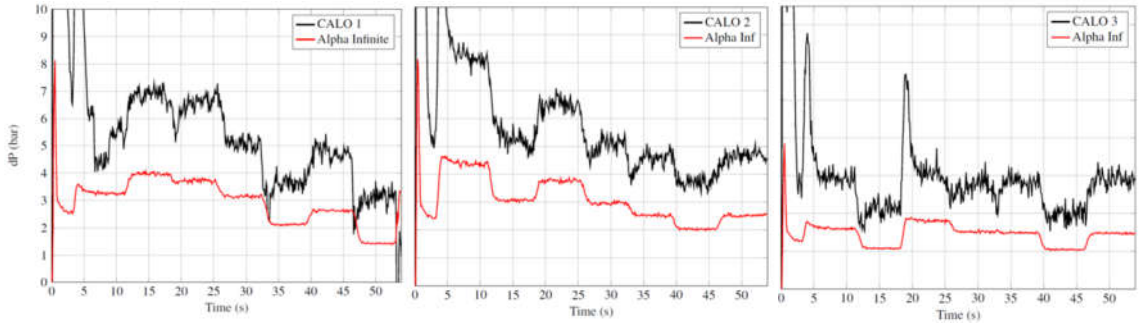


Figure 2: Comparison of test results of CALO 1, 2 and 3 with simulation using Alpha Infinite and Beta constant

The results, however, provide a pressure drop difference and standard deviation relatively low when compared to the chamber pressure range and total pressure drop, as shown at Table 2. Nevertheless, is important that the results precision be increased, which results in a requirement for more sophisticated models as is presented in this work.

Table 2 – Results of simulation using Alpha Infinite and Beta constant

| Load Point | Difference [bar] | Deviation [bar] | Deviation [%] |
|---|---|---|---|
| 1A | -1,71 | ±0,74 | -34,35 |
| 2A | -2,91 | ±0,27 | -42,29 |
| 3A | -2,84 | ±0,27 | -43,29 |
| 4A | -1,93 | ±0,24 | -38,03 |
| 5A | -1,50 | ±0,25 | -41,49 |
| 6A | -2,13 | ±0,25 | -44,74 |
| 7A | -1,76 | ±0,27 | -55,31 |
| 1B | -3,85 | ±0,27 | -46,76 |
| 2B | -0,84 | ±0,36 | -16,14 |
| 3B | -2,17 | ±0,27 | -33,16 |
| 4B | -0,72 | ±0,34 | -14,13 |
| 5B | -0,34 | ±0,52 | -7,49 |
| 6B | 0,37 | ±0,66 | -9,93 |
| 7B | -2,20 | ±0,18 | -46,66 |
| 1C | -2,70 | ±0,32 | -45,72 |
| 2C | -2,12 | ±0,38 | -49,71 |
| 3C | -2,58 | ±0,49 | -41,63 |
| 4C | -2,46 | ±0,47 | -44,88 |
| 5C | -2,71 | ±0,33 | -47,66 |
| 6C | -1,87 | ±0,42 | -47,39 |
| 7C | -2,91 | ±0,35 | -49,70 |

### 4.2. Alpha Infinite with Beta Variable

The improvement of the results using beta variable are considerable, despite the absence of the term for alpha, as shown in Figure 3.

DOI: 10.13009/EUCASS2019-528



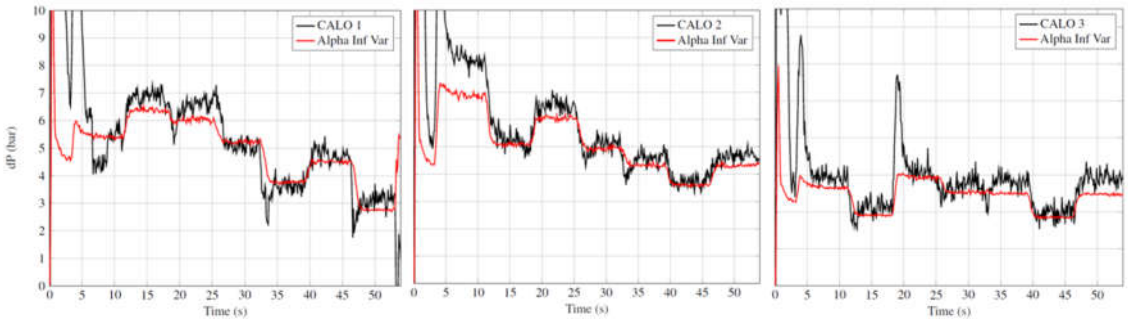


Figure 3: Comparison of test results of CALO 1, 2 and 3 with simulation using Alpha Infinite and Beta Variable

However, despite the difference and deviation be lower when compared to the 4.1, the dispersion of the results is still elevated when compared to the models which use alpha term to describe the viscosity effects. The main parameters are presented at the Table 3.

Table 3– Results of simulation using

| Load Point | Difference [bar] | Deviation [bar] | Deviation [%] |
|---|---|---|---|
| 1A | 0,45 | ±0,75 | 9,07 |
| 2A | -0,51 | ±0,29 | -7,40 |
| 3A | -0,53 | ±0,29 | -8,09 |
| 4A | 0,15 | ±0,26 | 2,96 |
| 5A | 0,15 | ±0,26 | 4,02 |
| 6A | -0,24 | ±0,26 | -5,11 |
| 7A | -0,43 | ±0,28 | -13,56 |
| 1B | -1,33 | ±0,29 | -16,20 |
| 2B | -0,12 | ±0,33 | -2,38 |
| 3B | -0,48 | ±0,28 | -7,33 |
| 4B | -0,13 | ±0,31 | -2,60 |
| 5B | -0,26 | ±0,26 | -5,59 |
| 6B | -0,12 | ±0,24 | -3,23 |
| 7B | -0,40 | ±0,18 | -8,54 |
| 1C | -0,57 | ±0,34 | -9,71 |
| 2C | -0,45 | ±0,39 | -10,49 |
| 3C | -0,32 | ±0,51 | -5,24 |
| 4C | -0,44 | ±0,48 | -7,99 |
| 5C | -0,69 | ±0,34 | -12,09 |
| 6C | -0,26 | ±0,43 | -6,49 |
| 7C | -0,90 | ±0,37 | -15,46 |

### 4.3. Alpha and Beta with Beta Variable

The improvement of this model, when compared to the 4.2 is more evident at the transient behavior for operation conditions changes, as is possible to identify at Figure 4

DOI: 10.13009/EUCASS2019-528



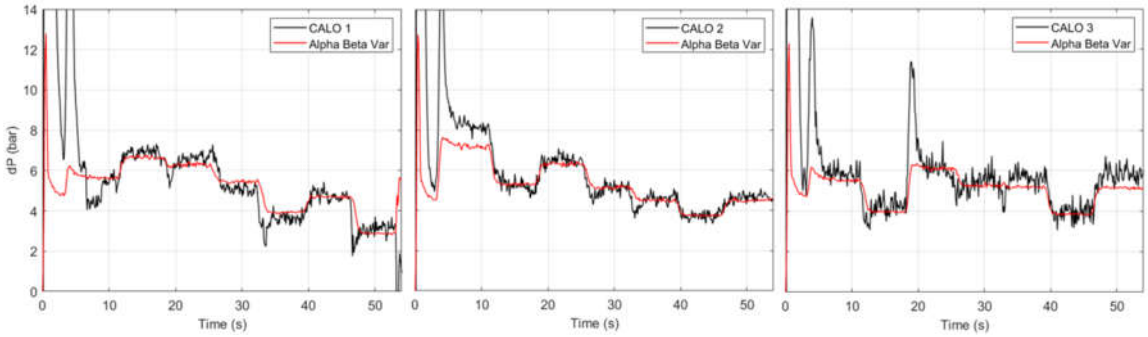


Figure 4: Comparison of test results of CALO 1, 2 and 3 with simulation using Alpha and Beta with Beta Variable

Is important to clarify that the reason for load point 1A, 1B as well as the pressure peak and pressure dip during operation conditions changes are not fully understood and the current hypothesis indicates as transport phenomena due to different time constants associated to mass flow rate measurement and fluid properties information at such location. At Table 4 is possible to identify these deviation peaks and dips.

Table 4– Results of simulation using Alpha and Beta with Beta Variable

| Load Point | Difference [bar] | Deviation [bar] | Deviation [%] |
|---|---|---|---|
| 1A | 0,68 | ±0,75 | 13,64 |
| 2A | -0,24 | ±0,29 | -3,46 |
| 3A | -0,28 | ±0,29 | -4,25 |
| 4A | 0,37 | ±0,26 | 7,29 |
| 5A | 0,30 | ±0,27 | 8,34 |
| 6A | -0,06 | ±0,27 | -1,22 |
| 7A | -0,31 | ±0,28 | -9,73 |
| 1B | -1,03 | ±0,30 | -12,58 |
| 2B | 0,09 | ±0,34 | 1,72 |
| 3B | -0,22 | ±0,28 | -3,37 |
| 4B | 0,07 | ±0,31 | 1,46 |
| 5B | -0,08 | ±0,27 | -1,71 |
| 6B | 0,03 | ±0,24 | 0,79 |
| 7B | -0,23 | ±0,19 | -4,77 |
| 1C | -0,35 | ±0,34 | -5,94 |
| 2C | -0,29 | ±0,39 | -6,77 |
| 3C | -0,07 | ±0,51 | -1,20 |
| 4C | -0,23 | ±0,49 | -4,17 |
| 5C | -0,48 | ±0,34 | -8,49 |
| 6C | -0,10 | ±0,43 | -2,61 |
| 7C | -0,70 | ±0,37 | -12,00 |

### 4.4. Carman-Kozeny

The use of Carman-Kozeny standard parameters shows a reduction of the precision, despite a more complex model when compared to the previous attempts, as presented at Figure 5.

DOI: 10.13009/EUCASS2019-528



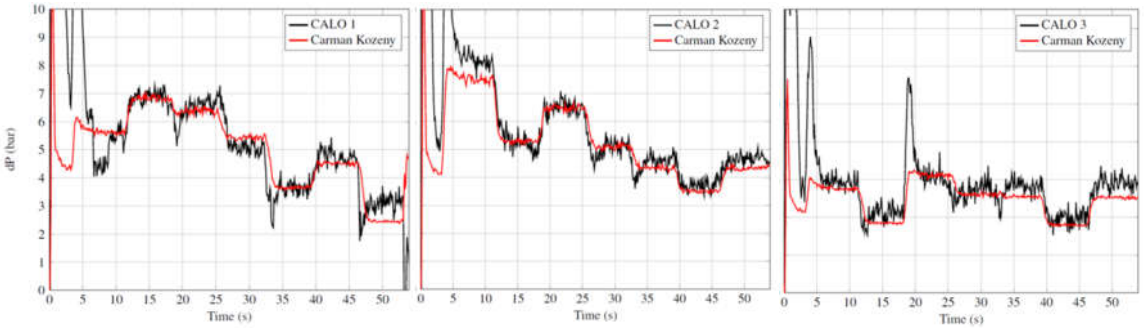


Figure 5: Comparison of test results of CALO 1, 2 and 3 with simulation using Carman-Kozeny

Also, despite the pressure drop difference shows a low range at Table 5, the dispersion of the deviation is not consistent with expected precision required for a broad range of operation conditions target for this model implementation at the frame of cycle analysis as well as design.

Table 5– Results of simulation using Carman-Kozeny model

| Load Point | Difference [bar] | Deviation [bar] | Deviation [%] |
|---|---|---|---|
| 1A | 0,66 | ±0,76 | 13,25 |
| 2A | -0,05 | ±0,30 | -0,78 |
| 3A | -0,18 | ±0,31 | -2,78 |
| 4A | 0,35 | ±0,27 | 6,98 |
| 5A | 0,03 | ±0,27 | 0,95 |
| 6A | -0,24 | ±0,27 | -5,02 |
| 7A | -0,74 | ±0,28 | -23,25 |
| 1B | -0,71 | ±0,31 | -8,6 |
| 2B | 0,08 | ±0,34 | 1,48 |
| 3B | -0,04 | ±0,29 | -0,66 |
| 4B | 0,03 | ±0,32 | 0,61 |
| 5B | -0,24 | ±0,27 | -5,28 |
| 6B | -0,22 | ±0,24 | -5,79 |
| 7B | -0,39 | ±0,19 | -8,23 |
| 1C | -0,37 | ±0,34 | -6,33 |
| 2C | -0,56 | ±0,40 | -13,26 |
| 3C | 0,05 | ±0,52 | 0,84 |
| 4C | -0,28 | ±0,49 | -5,10 |
| 5C | -0,58 | ±0,35 | -10,26 |
| 6C | -0,36 | ±0,44 | -9,19 |
| 7C | -0,80 | ±0,37 | -13,75 |

## 4.5. Carman-Kozeny with $CK_{f2}$ Variable

The use of Carman-Kozeny with Reynolds dependent $CK_{f2}$ indicates an improvement when compared with previous simulations as show previously at this work. The dynamical behavior of pressure drop, as shown on Figure 6 indicated a promising methodology for this system analysis in non-stationary form.

DOI: 10.13009/EUCASS2019-528



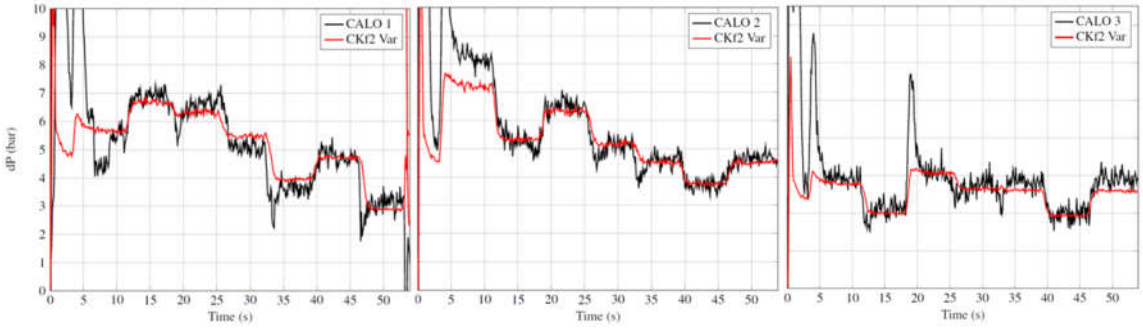


Figure 6: Comparison of test results of CALO 1, 2 and 3 with simulation using Carman-Kozeny and $CK_{f2}$ variable

The deviation, when compared with all the previous models shows a minor improvement, indicating the possible limit of precision of this method with regarding of the measurements system used. The dispersion of pressure deviation is minor as show on Table 6.

Table 6– Results of simulation using Carman-Kozeny and $CK_{f2}$ variable

| Load Point | Difference [bar] | Deviation [bar] | Deviation [%] |
|---|---|---|---|
| 1A | 0,71 | ±0,75 | 14,27 |
| 2A | -0,21 | ±0,29 | -3,01 |
| 3A | -0,25 | ±0,29 | -3,77 |
| 4A | 0,40 | ±0,26 | 7,87 |
| 5A | 0,32 | ±0,27 | 8,95 |
| 6A | -0,03 | ±0,27 | -0,65 |
| 7A | -0,30 | ±0,28 | -9,55 |
| 1B | -1,01 | ±0,30 | -12,23 |
| 2B | 0,12 | ±0,33 | 2,28 |
| 3B | -0,19 | ±0,28 | -2,92 |
| 4B | 0,10 | ±0,31 | 2,03 |
| 5B | -0,05 | ±0,27 | -1,14 |
| 6B | 0,05 | ±0,24 | 1,36 |
| 7B | -0,20 | ±0,19 | -4,22 |
| 1C | -0,32 | ±0,34 | -5,41 |
| 2C | -0,27 | ±0,39 | -6,25 |
| 3C | -0,04 | ±0,51 | -0,72 |
| 4C | -0,20 | ±0,49 | -3,63 |
| 5C | -0,45 | ±0,34 | -7,98 |
| 6C | -0,08 | ±0,43 | -2,06 |
| 7C | -0,67 | ±0,37 | -11,49 |

## 4.6. Reynold dependence

The Reynolds dependence approach results in a simplification of transient models with minor perceptual deviation when compared to the previous transient simulations. As is possible to see at Figure 7, the transient behavior between multiple loads points are improved when compared to Carman-Kozeny using variable $CK_{f2}$.

DOI: 10.13009/EUCASS2019-528



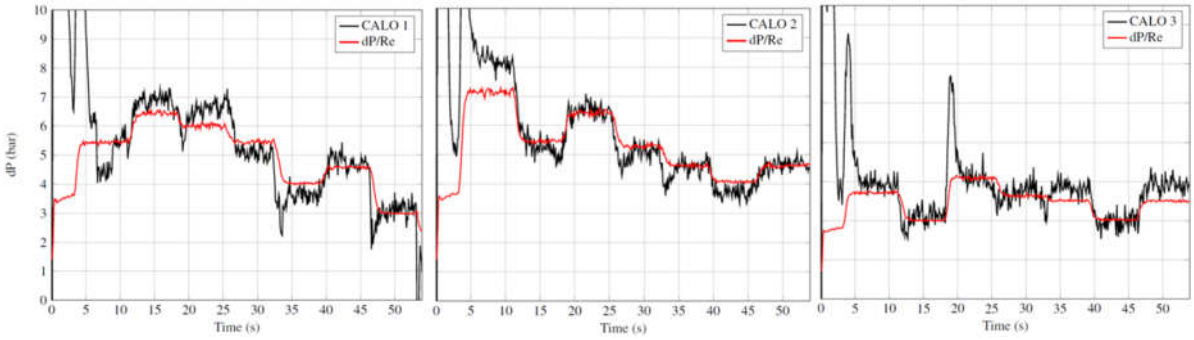


Figure 7: Comparison of test results of CALO 1, 2 and 3 with simulation using Reynold dependence at EcosimPro

As is possible to see at the Table 7, the overall deviation is relatively small, but the dispersion of the absolute difference is degraded when compared to the use of other models. The possible main reason of such errors could be associated to the absence of further information of geometrical properties.

Table 7– Results of simulation using Reynold dependence

| Load Point | Difference [bar] | Deviation [bar] | Deviation [%] |
|---|---|---|---|
| 1A | 0,46 | ±0,74 | 9,33 |
| 2A | -0,45 | ±0,28 | -6,48 |
| 3A | -0,55 | ±0,28 | -8,44 |
| 4A | 0,38 | ±0,25 | 7,44 |
| 5A | 0,41 | ±0,26 | 11,29 |
| 6A | -0,17 | ±0,25 | -3,56 |
| 7A | -0,20 | ±0,27 | -6,30 |
| 1B | -1,08 | ±0,28 | -13,15 |
| 2B | 0,25 | ±0,33 | 4,80 |
| 3B | -0,10 | ±0,27 | -1,53 |
| 4B | 0,23 | ±0,30 | 4,51 |
| 5B | 0,05 | ±0,26 | 1,02 |
| 6B | 0,36 | ±0,23 | 9,57 |
| 7B | -0,10 | ±0,18 | -2,04 |
| 1C | -0,48 | ±0,32 | -8,12 |
| 2C | -0,25 | ±0,38 | -5,91 |
| 3C | -0,02 | ±0,49 | -0,34 |
| 4C | -0,23 | ±0,48 | -4,13 |
| 5C | -0,66 | ±0,34 | -11,57 |
| 6C | 0,09 | ±0,42 | 2,23 |
| 7C | -0,85 | ±0,36 | -14,48 |

## 5. LUMEN Demonstrator

Due its high performance when compared to standard shear-coaxial injectors as well as its axial heat release improvement, the use of API is advantageous for expander bleed cycle are preferable. As for LUMEN demonstrator, the possibility to use the API is also driven by the heritage of DLR technology of such injector design.
With operational envelope for combustion chamber pressure between 3,5MPa and 8,0MPa, the injection conditions requires LNG injection temperature above 200K in order to avoid phase change at the injector head [14][15]. Also, the porous face plate, which will cover the entire chamber cross section of 80mm diameter, is foreseen to be divided into three plates of sintered steel mesh with 12mm thickness each [15], similar as the material used for the test cases presented in this work.
Thus, the utilization of LNG (i.e., the different fluid) shall be the major difference for the expected results and simulations. Nevertheless, the current models are been adjusted to perform the first prediction of operational conditions at steady-state phase as well as the transient analysis of LUMEN demonstrator.

DOI: 10.13009/EUCASS2019-528



## 6. Conclusion

The standard models for flow analysis through porous media requires improvements in order to be able to evaluate the operating conditions regarding a LRE porous injection system in steady-state as well in transient operation. However, even with the flow dependent parameters which were initially adopted as constant, some transient phenomena, especially during ignition conditions presented strong deviation. The possible cause of this uncertainty could be related to the transport characteristics of fluid through the porous media, where a more precise modeling of cavities can improve these results.
For a representative transient for LUMEN demonstrator, not only Methane fluid must be validates, as well as the node discretization of porous path will improve the transient analysis due to improved precision at phase change conditions. Liquid phase behavior though porous injector system wasn't part of this works, but will be necessary for validation of the proposed models in a broad operation range.
Nevertheless, improvement of Carman-Kozeny allows reducing the associated errors, while Reynold dependency model provides a good approach for analysis of transient. However, this approach needs to be deeply investigated to identify the geometrical parameters for the correlation in order to mitigate the error propagation and be able to predict the flow dynamic behavior without needs for previously experimental data.
The current information, however allows having a minimum error deviation when compared with previous models, making the initial prediction of transient and steady-state conditions of LUMEN Demonstrator more accurate than previously expected.

## 7. Future works

As proposal for future works, an in detail investigation of Methane in gaseous and liquid form, at subcritical, transcritical and supercritical conditions will heavily improve the knowledge of flow behavior and dynamic characteristics of the Advanced Porous Injector at flow conditions compatible with LRE operating conditions.
Adjustment of Reynolds dependency according to geometrical properties will be carefully evaluated in order to identify possible dependences and target the improvement of transient prediction of API devices applied to LRE. Furthermore, the implementation of multiple nodes analysis for investigation of phase change and heat transfer was identified as a important step toward more physically correct analysis for LUMEN Demonstrator as well as for expander bleed cycle engine and API device.

## 8. Acknowledgement

The authors would like to thank all DLR personnel involved in the CALO test campaign, the P8 team, and manufacturing process. Special thanks to the LUMEN Demonstrator Team and everyone involved in the progress of propulsion system of DLR.

## References

[1] Deeken, J. C., Suslov, D., Rackemann, N., Preuss, A. 2014. Combustion Performance and Stability of a Porous Injector Compared with a State-of-the-Art Coaxial Injector. Space Propulsion 2014.
[2] Deeken, J., Suslov, D., Haidn, O., Schlechtriem, S. 2010. Design and Testing of a Porous Injector Head for Transpiration Cooled Combustion Chambers. AIAA.
[3] Deeken, J., Suslov, D., Schlechtriem, S., Haidn, O. 2011. Impact of Injection Distribution on Cryogenic Rocket Engine Stability. 4th EUCASS
[4] Negoro, N., Ogawara, A., Onga, T., Manako, H., Kurosu, A., Yamanishi, N., Miyazaki, K., Hori, S., Okita, K. and Kumakawa, A. 2007. Next Booster Engine LE-X in Japan, AIAA Paper 2007-5490
[5] Atsumi, M, et al. 2011. Development of the LE-X Engine. Mitsubishi Heavy Industries Technical Review Vol. 48 No. 4.
[6] Yanagawa, K., Fujita, T., Miyajima, H., Kishimoto, K. 1985. High-Altitude Simulation Tests of the LOx/LH2 Engine LE-5. J. Propulsion.

DOI: 10.13009/EUCASS2019-528



[7] Schmidt, B. E. 2014. Compressible Flow Through Porous Media with Application to Injection. Tech. rep. California Institute of Technology.
[8] Tully, L. R. 2005. “Numerical Modeling Of Transpiration Cooled Rocket Injectors”. Ma Thesis. University of Florida.
[9] Fahd Siddiqui, Mohamed Y. Soliman. 2017. Non-Darcy Skin Effect with a New Boundary Condition. In: International Journal of Petroleum and Petrochemical Engineering 3.1
[10] Ruth, D., Ma, H. 1992. On the Derivation of the Forchheimer Equation by Means of the Averaging Theorem”. In: Transport in Porous Media 7: 255-264
[11] Macdonals, I. F., El-Sayed, M. S., Mow, K, Dullien F. A. L. 1979. Flow Through Porous Media - the Ergun Equation Revisited. In: Ind. Eng. Chem. Fundam., Vol. 18, No. 3
[12] Werling, L. K., Müller, S., Andreas Hauk, A., Ciezki, H. K., Schlechtriem, S. 2016. Pressure Drop Measurement of Porous Materials: Flashback Arrestors for a N2O/C2H4 Premixed Green Propellant”. Joint Propulsion Conference. AIAA
[13] Deeken, J., Suslov, D., Haidn, O., Schlechtriem, S. 2011. Combustion Efficiency Of A Porous Injector During Throttling Of A LOx/H2 Combustion Chamber. Progress in Propulsion Physics 2 (2011) 251-264
[14] Deeken, J., Oschwald, M., Schlechtriem, S. 2019. LUMEN Demonstrator – Project Overview. ISTS
[15] Hardi, J., Deeken, J., Armbuster, W., Miene, Y., Haemisch, J, Martin, J., Suslov, D., Oschwald, M. 2019. LUMEN Thrust Chamber – Injector Design and Stability Analysis. ISTS.